IEEE Access
Multidisciplinary | Rapid Review | Open Access Journal

Received May 24, 2021, accepted July 1, 2021, date of publication July 9, 2021, date of current version July 19, 2021.

Digital Object Identifier 10.1109/ACCESS.2021.3096047

Micropart Motion on a Surface Due to Controlled Surface Excitation

MUHAMMAD AHSAN NAEEM[1], MOHSIN RIZWAN[1,2], AND P. S. SHIAKOLAS[3]

[1]Mechatronics and Control Engineering Department, University of Engineering and Technology, Lahore, Lahore 54000, Pakistan
[2]Human-Centered Robotics Lab, National Center of Robotics and Automation (NCRA), Lahore 54000, Pakistan
[3]Mechanical and Aerospace Engineering Department, The University of Texas at Arlington, Arlington, TX 76019, USA

Corresponding author: Mohsin Rizwan (mohsin.rizwan@uet.edu.pk)

ABSTRACT Many types of devices and handling platforms are used for microscale manipulation and microassembly ranging from microgrippers for individual part handling to work surfaces equipped with discrete actuators capable of simultaneous multiple part handling and manipulation. Micropart handling using discrete actuators suffers from dead zone constraint that requires the size of the part to be larger than the gap between consecutive actuators to ensure part contact with multiple actuators at all times for proper handling. In the context of the dead zone constraint, a new micromanipulation technique was proposed in our previous work based on the concept of active deformable surface. The time-dependent deformation geometry of the micropart carrying surface is controlled by actuators rigidly attached to it. The deformation acceleration imparted by the actuators generates an inertia which, considering other parameters, can induce a motion on the micropart placed on the surface. These parameters include size, mass and material properties of the micropart and the surface roughness characteristics. This research extends our previous work of modeling micropart dynamics and motion from 1D to motion on a 2D surface. The mathematical model is developed and subsequently employed in numerical simulations to study the micropart motion and controlled translocation on the deformable active surface. The analysis allows for the identification of a feasible region of influence of the actuator, effects of surface motion characteristics, micropart convergence at particular locations and evaluation of motion characteristics. The results of this research could be advantageously employed for the development of 2D microconveyors as an integral component of microassembly platforms.

INDEX TERMS 2D active surface, continuous actuation, microconveyor, microscale forces, microscale motion, MEMS.

I. INTRODUCTION

The history of micropart handling goes back to the conception and production of micro electromechanical systems (MEMS). Small scale devices can perform not only similar tasks as macroscale machines but achieve additional functionality due to smaller inertia, larger surface forces and smaller footprint. MEMS production mostly comprises of two steps: microscale component manufacturing and assembly. Assembly in general and at microscale usually comprises of two stages of position and placement. Various types of machines are used for microscale handling which can be categorized into two groups.

- Pick and Place Devices: These include various types of microgrippers including electromechanical [1], electrothermal [2], acoustic [3] and optical tweezers [4], [5].
- Part handling workcells: These workcells, comprising of an array of actuators, are used to translocate the part at the required location. Various types of actuators are used on these workcells including ultrasonic [6], thermobimorph [7], compressed air nozzles [8], air-levitated electrically driven platforms [9], electrostatic attraction-repulsion mechanisms [10], microconveyor comprising of discrete microblocks containing microcontroller, sensors and microactuators [11], [12], and a conveyor-based bridge resonator driven by linear traveling waves with the support of 3D printed legs [13]. A concept of controlling the motion of multiple objects on a Chladni plate is presented in [14], however, no model discussing the interaction of microscale forces between particle and surface is presented.

These part handling workcells, due to their discrete actuation mechanisms, are limited in their ability or unable to

The associate editor coordinating the review of this manuscript and approving it for publication was Yue Zhang.

handle microscale components mainly due to the dead zone constraint. This constraint requires the micropart dimension to be larger than the free space between two consecutive actuators as shown schematically for a pneumatic microconveyor in Fig. 1a [15], otherwise the micropart could get trapped in the free space. To address the limitation on microactuator spacing and part dimensions, the concept of active surface was proposed [16]. The conceptual schematic of the active surface is shown in Fig. 1b & c. The proposed methodology has the advantage that controlled motion is possible even if the particle size is smaller than the actuator spacing. A micropart carrying surface is controllably deformed using rigidly attached actuators thus inducing controlled acceleration to the micropart on the surface. The induced acceleration component perpendicular to the surface will push (repel) or pull (attract) the micropart away or towards the surface based on surface roughness and other characteristics effectively changing the friction force between the micropart and the surface. The acceleration component parallel to the surface affects the translocation characteristics of the micropart on the active surface.

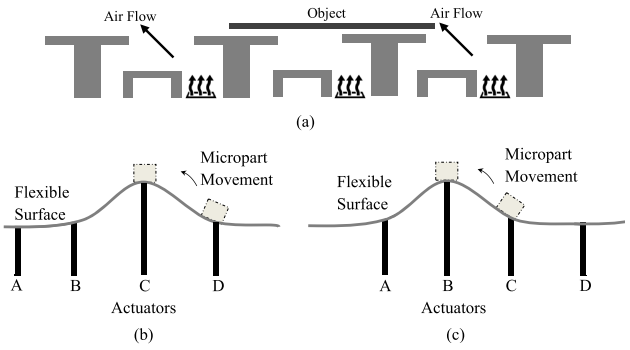

FIGURE 1. (a) Discrete-actuator we-actuator workcell with dead zone [15] and (b,c) Microconveyor using flexible surface providing continuous actuation [16].

The 1D analysis of the active surface concluded that the micropart motion is a function of input frequency and amplitude of actuation, surface roughness, material properties, and spacing of actuators [17]. It was also found that motion is only feasible within a range of frequencies; the micropart detaches from the surface at higher frequencies whereas motion is not feasible below a lower threshold value of frequency.

In the current research, the 1D active surface microconveyor analysis is extended to 2D towards the development of a microconveyor surface. The mathematical model is developed and presented. Subsequently, considering micropart and surface properties, a simulation algorithm is proposed and verified using benchmark cases. The details of the numerical scheme based on the developed mathematical model are presented along with the motion analysis. The manuscript closes with a discussion on micropart position convergence at particular locations on the workcell surface.

II. MATHEMATICAL MODEL

The mathematical model of micropart motion is developed considering micropart, active surface and actuator parameters, and dominant forces at microscale. The large surface area to volume ratio and resultant dominant surface forces are the most significant differences between macro- and microscale motion dynamics [18], [19]. At the microscale, surface forces are a strong function of material properties and the average distance between the two surfaces [20]. The motion dynamics are developed using the summation of surface forces (including the attraction and repulsion due to compression of asperities), friction force and inertia due to the applied acceleration on the flexible active surface. We have used MATLAB to code and simulate the model. The details of system definition, inputs and evaluation of friction forces are introduced and discussed in the following subsections.

A. SURFACE DEFORMATION PROFILE

The active surface deformation profile used in this research is assumed to be that of an elastic thin plate with clamped ends and an applied force, P, at its center. The deformation geometry is evaluated according to classical solutions in plate bending theory [21]. The deformation equation of a circular plate of diameter D with clamped ends in a cylindrical coordinate system is given by

$$\frac{d}{dr}\left[\frac{1}{r}\frac{d}{dr}\left(r\frac{dw}{dr}\right)\right] = -\frac{Q}{D} \tag{1}$$

and the solution with clamped boundary conditions is given by

$$w = \frac{P}{16\pi D}\left(2r^2 \ln\left(\frac{r}{a}\right) + a^2 - r^2\right) \tag{2}$$

where w is the vertical deflection at radius r, Q is the shear force and a is the maximum radius of the plate.

B. SYSTEM INPUTS

The active surface is assumed to be deformed by piezo-actuators located below the surface and rigidly attached to it. The piezo-actuators provide the controlled input characteristics. A quintic input motion profile is used with predefined acceleration and jerk control [16]. The motion profile assumes zero velocity and acceleration at the initial and final position states.

C. SURFACE AND FRICTION FORCES

Various models have been proposed in the open literature to relate the surface forces and microscale nonlinear friction force to surface roughness and material properties. Kogut and Etsion proposed a model (KE model) based on finite element analysis results of single asperity contact and extended it to multi-asperity contact [20], [22]–[24]. Similar to our previous work, the multi-asperity KE model is employed to estimate the nonlinear friction force and coefficient of friction which dynamically varies with change in the normal force [25]. The surface and friction forces are estimated using the equations

developed in our previous research [16] and are presented here in (3), (4) and (5) for completeness.

$$P = \frac{2}{3} HA_n \pi \beta \frac{\omega_c}{\sigma} \left(\int_{d}^{d+\omega_c} I^{1.5} + 1.03 \int_{d+\omega_c}^{d+6\omega_c} I^{1.425} + 1.4 \int_{d+6\omega_c}^{d+110\omega_c} I^{1.263} + \frac{3}{K} \int_{d+110\omega_c}^{\infty} I \right) \tag{3}$$

$$F_s = 2\, HA_n \pi \beta \theta \left(\int_{-\infty}^{d} J_{nc} + 0.98 \int_{d}^{d+\omega_c} J_{-0.29}^{0.298} + 0.79 \int_{d+\omega_c}^{d+6\omega_c} J_{-0.321}^{0.356} + 1.19 \int_{d+6\omega_c}^{d+110\omega_c} J_{-0.332}^{0.093} \right) \tag{4}$$

$$Q_{max} = \frac{2}{3} HA_n \pi \beta K \frac{\omega_c}{\sigma} \left(0.52 \int_{d}^{d+\omega_c} I^{0.982} + \int_{d+\omega_c}^{d+6\omega_c} (-0.01 I^{4.425} + 0.09 I^{3.425} - 0.4 I^{2.425} + 0.85 I^{1.425}) \right) \tag{5}$$

where $J_{nc} = \frac{4}{3}\left[\left(\frac{\epsilon}{d-z} \right)^2 - 0.25 \left(\frac{\epsilon}{d-z} \right)^8 \right] \varphi_z dz$, $J_c^b = \left(\frac{z-d}{\omega_c} \right)^b \left(\frac{\epsilon}{\omega_c} \right)^c \varphi_z dz$, and $I^b = \left(\frac{z-d}{\omega_c} \right)^b \varphi_z dz$

The KE model uses the mean distance between two rough surfaces, material properties and surface roughness to estimate the repulsion force due to asperities compression and attraction between two surfaces due to surface forces and nonlinear friction force. However, in a dynamic environment, like the one considered in this research, the attraction and friction forces between the surfaces in contact must be continuously evaluated while the external forces are known. In order to evaluate these forces, the KE model must be continuously inverted to calculate the mean distance between the surfaces in contact as a function of the external force input. The details of using the KE model in a dynamic simulation are thoroughly presented in our previous research [16] and in the interest of space of the present manuscript will not be repeated here. Even though capillary and electrostatic forces could be dominant at microscale with well defined mathematical models, their magnitudes in a controlled environment with very low relative humidity and a grounded workcell similar to the environment considered in this research, are negligible [18], [26]–[28] and they will not be considered in this research work.

D. SYSTEM DYNAMICS

The system dynamics are modeled by estimating the instantaneous value of inertia imparted to the micropart. This inertia has components parallel and perpendicular to the active surface and is a result of actuator input motion characteristics. The component parallel to the surface while considering the friction force influences the motion of micropart along the surface, whereas the perpendicular component affects the vertical mean distance of the micropart relative to the surface (repulsion/attraction) and used to dynamically evaluate the coefficient of friction and friction force. The dominant forces for microscale dynamics are shown in Fig. 2, where A_{cc} is the direction of imparted acceleration, I_T is the generated inertia with components parallel, I_{prl}, and perpendicular, I_{perp}, to the surface. F_s is the attraction force, P is the repulsion force and F_{net} is the resultant net force acting on the surface by the micropart.

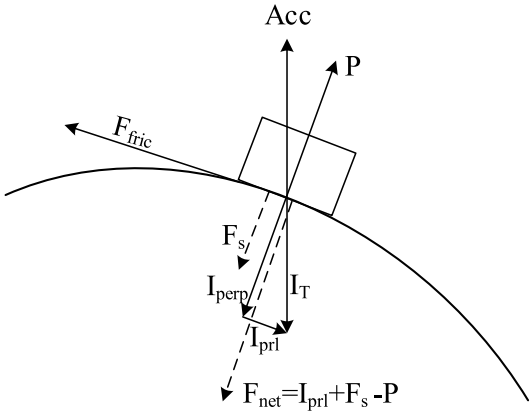

FIGURE 2. Schematic of the forces on the micropart placed on the base surface.

The friction force is not just the function of net force, F_{net}, but a function of system states as well. Its magnitude is equal to the external force if there is no relative movement between the surfaces in contact, and is at its maximum value if the surfaces in contact are slipping or at the verge of slipping relative to each other. Its direction is opposite to the direction of relative velocity between the two surfaces in contact. The non-linearity of the friction force is presented in Fig. 3.

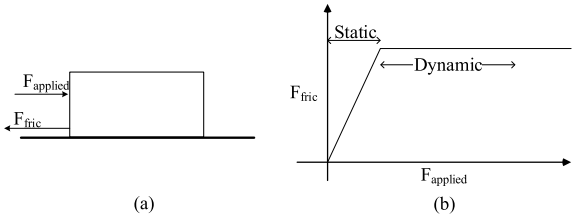

FIGURE 3. Change of friction with applied load for constant friction factor.

A friction logic algorithm is developed to estimate the friction force (magnitude and direction) in this dynamic environment considering the system state and the value of maximum possible friction force. As the relative velocity between the surfaces in contact changes direction, there must be a condition of sticking between the two surfaces, i.e. the micropart will stop relative to the surface. A threshold velocity is introduced to capture the stick-slip behavior of the micropart in motion. The threshold velocity, V_T, is defined as the magnitude of the relative velocity, V_r, which within one integration time step, Δt, will become zero under the influence of the instantaneous value of friction force, F_f as

shown in (6).

$$F_f = ma \quad a = \frac{V_T - 0}{\Delta t} \quad V_T = \left(\frac{F_f}{m}\right)\Delta t \tag{6}$$

where m is micropart mass and a is the base surface acceleration.

Once the threshold velocity is estimated, the friction logic algorithm which allows for the evaluation of the micropart acceleration is mathematically presented in (7).

$$if\ V_r \geq V_T\ then\ \ddot{X} = \frac{F_e}{m} \tag{7a}$$

$$elseif\ V_r \leq V_T\ and\ F_e > F_f\ then\ \ddot{X} = \frac{F_e}{m} \tag{7b}$$

$$else\ \ddot{X} = a \tag{7c}$$

where F_e is the net external applied force and $\ddot{X}$ is the acceleration of the micropart.

The performance of the friction logic algorithm is evaluated by simulating the motion of a micropart on a surface (platform) under a constant coefficient of friction while the surface is undergoing a sinusoidal motion of varying amplitude. The oscillatory motion of the platform was chosen since it causes reversal of its direction of motion and the varying amplitude induces a range of acceleration values. The velocities of the part and surface, and their difference due to the oscillatory platform motion are presented in Fig. 4. The base surface and the part move with the same velocity during the initial phase. Once the inertia becomes larger (due to larger amplitude of oscillation) than the friction force, the part starts sliding relative to the surface at 2.41 s. Subsequently, when the base surface starts moving in the opposite direction, the part sticks to the surface momentarily at 2.87 s, reverses its motion and slides in the opposite direction following the motion of the surface. The part velocity follows the surface velocity until the initiation of slip, and afterwards, the part velocity follows a straight line profile with constant acceleration due to constant friction force. The relative velocity, shown by the solid line in Fig. 4, becomes zero at every reversal of base surface velocity, which indicates that the algorithm successfully captures the effect of variation of friction force and stick-slip behavior.

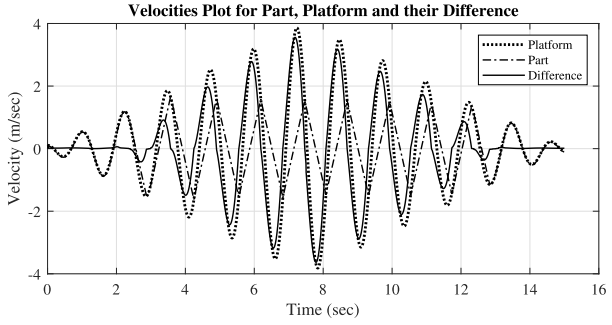

FIGURE 4. Friction logic verification: Input is the surface displacement as function of time and output is the resultant displacement of part resting on oscillating surface.

III. MOTION FEASIBILITY

Motion is induced on the micropart by imparting high acceleration through the base surface. The component of inertia parallel to the surface (considering the friction force) causes the motion of the micropart along the surface. The motion feasibility is established by comparing the parallel component of inertia I_{prl} with the corresponding friction force which is a function of F_{net} as shown in Fig. 2. The feasible area for motion is the surface area within the influence of an actuator; when F_{fric} is less than I_{prl}, sliding motion is generated and I_{perp} is less than F_s so as to avoid detachment. The surface could be deformed at different frequencies and amplitudes, and requires the evaluation of the instantaneous value of I_{perp} and corresponding F_{fric}. The feasible area is estimated for various values of actuator stroke length over a range of actuator frequencies. The variation of the feasible area with input frequency is shown in Fig. 5 where the lower frequency threshold of approximately 200 Hz causes no movement for three different stroke lengths (h_f). For every stroke length, the feasible area increases with an increase in input frequency and starts decreasing after reaching its corresponding peak value. A decrease in the feasible area at higher frequencies is due to the large value of I_{perp} compared to the force of attraction (F_s) which causes the micropart to detach from the surface instead of sliding on it.

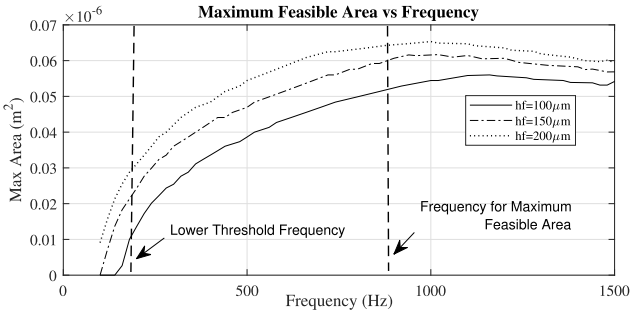

FIGURE 5. Variation of maximum feasible area with change of input frequency.

In addition, since the sliding motion between the micropart and surface is generated when I_{prl} exceeds F_f (the instantaneous value of F_{fric}) during one stroke, the longer I_{prl} is larger than F_{fric} the higher the likelihood of motion. Fig. 6 shows the time integral of the feasible area with the change in actuator frequency for various stroke lengths (h_f). The time integral of the feasible area is maximum around 300 to 400 Hz for various stroke lengths. Considering Fig. 5 and Fig. 6, the feasible range of frequencies is estimated to be between 300 to 1000 Hz and almost independent of stroke length h_f.

IV. MICROPART MOTION TRACKING ON SURFACE

A. ESTIMATION OF STATE UPDATING

The micropart motion due to controlled surface excitation is estimated using a custom developed numerical scheme. The magnitude and direction of the friction force are a function of relative velocity between the surface and micropart. Contrary

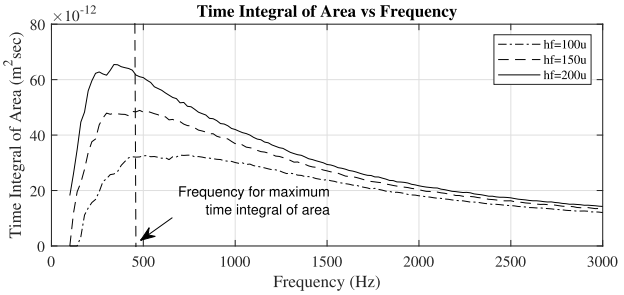

FIGURE 6. Time integral of feasible area with change of input frequency.

to this, the imparted inertia depends on the absolute value of stroke acceleration. To accommodate these relative and absolute quantities, two coordinate systems are introduced; a fixed global coordinate system (X, Y), and a local coordinate system (X_L, Y_L), as shown in Fig. 7. The local system is attached on the micropart and moves and orients with it. The orientation conversion between the two systems is performed using 3D rotation matrices.

The velocity of the micropart is transformed from global to local coordinates. The X-axis of the local coordinate system is always along the gradient of the surface at the instantaneous location of the micropart. The parameters used to describe the micropart motion are shown in Fig. 7. The dotted lines represent a circular topography of the active surface deformation due to a single actuator. β is the angle of rotation from the original location to the instantaneous location of micropart in global coordinates. γ is the angle of the instantaneous velocity of micropart with respect to X_L. The gradient of the surface at the current micropart location is represented by angle θ. The transformation matrix between the fixed and local systems is a function of β and θ and is presented in (8).

$$\begin{bmatrix} X_L \\ Y_L \\ Z_L \end{bmatrix} = \begin{bmatrix} c\theta c\beta & c\theta s\beta & s\theta \\ -s\beta & c\beta & 0 \\ -s\theta c\beta & -s\theta s\beta & c\theta \end{bmatrix} \begin{bmatrix} X \\ Y \\ Z \end{bmatrix} \tag{8}$$

where $cq = \cos q$ and $sq = \sin q$.

The motion of the micropart is estimated in the fixed global coordinates. At the instantaneous location of the micropart, the surface gradient is evaluated and the relative velocity of micropart with respect to the surface is calculated. The direction of the friction force is opposite to that of relative velocity. The component of the friction force in local coordinates is calculated and used to calculate acceleration along and perpendicular to the surface gradient. The stick-slip behavior is evaluated using the relative velocity of micropart with surface where the increment in absolute velocity is calculated along the local coordinates. Afterwards, these velocities are transformed to global coordinates and the micropart global position is updated.

Along the local coordinates, the increment in position and velocity are estimated by integrating the velocity and acceleration respectively and considering the surface gradient (θ) at the current micropart location. The orthogonal components of micropart velocity on a curved surface are shown in Fig. 8 where R represents the radius of curvature with subscripts x and y representing abscissa and ordinate respectively, ψ is the angle traced by the tangential component of velocity, V and a represent velocity and acceleration and Δ is the change in the state along a given coordinate. A first-order approximation for change in position and velocity of the micropart motion on a curved surface is represented by the mathematical relationships in (9) and graphically shown in Fig. 9.

$$\Delta X_L = R_x \sin \psi_x \tag{9a}$$
$$\Delta Y_L = R_Y \sin \psi_y \tag{9b}$$
$$\Delta Z_L = -sgn(R_x)(1 - \cos \psi_x)R_x - sgn(R_y)(1 - \cos \psi_y)R_y \tag{9c}$$

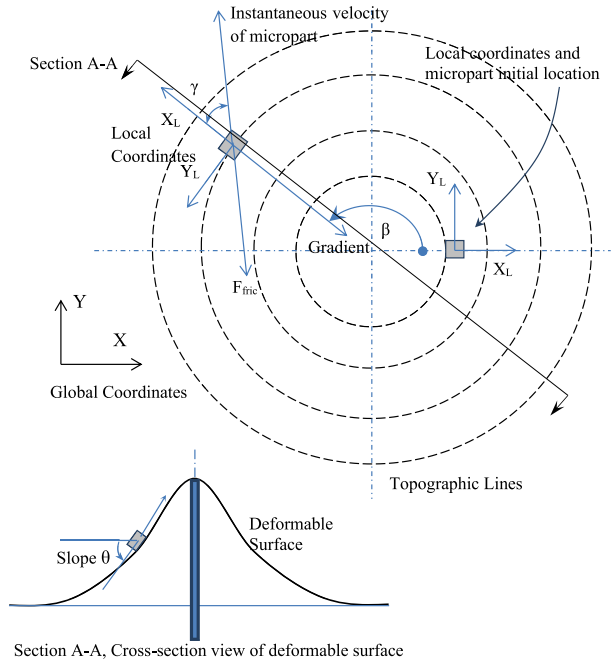

FIGURE 7. Global and local coordinates and movement directions.

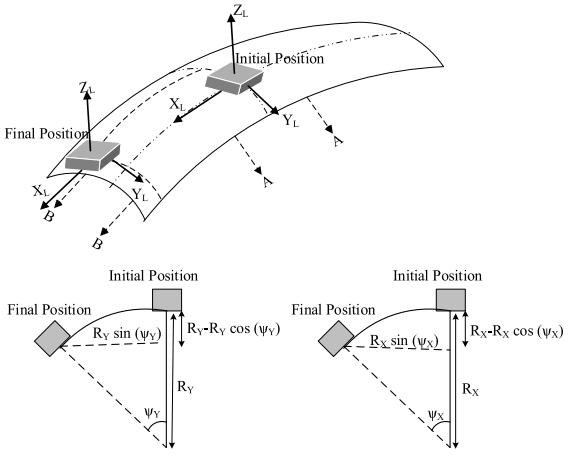

FIGURE 8. Micropart motion on a curved surface.

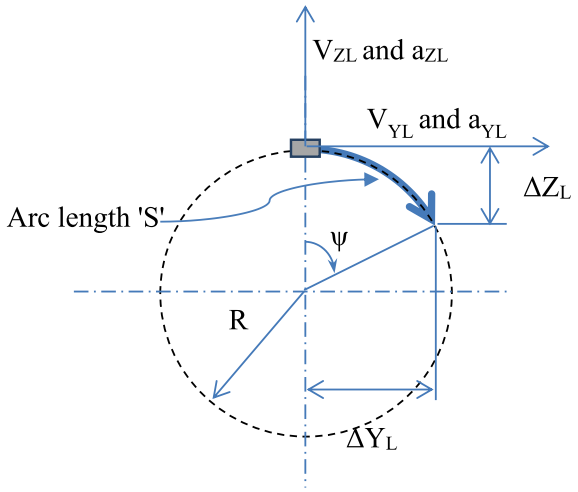

FIGURE 9. Position and velocity increment in local coordinates.

For the symmetric surface deformation profile as formed by the single point deformation of a plate, the equations of motion in state variable format for position updates can be approximated for small surface gradient as in (10).

$$\Delta X_L = V_r dt = V_{XL} dt \tag{10a}$$

$$\Delta Y_L = V_t dt = \left[\frac{R}{(\sin\theta)\, dt} \sin\left(V_{YL} \frac{(\sin\theta)\, dt}{R}\right)\right] dt \tag{10b}$$

$$\Delta Z_L = V_z dt = -\frac{R}{(\sin\theta)\, dt}\left[1 - \cos\left(V_{YL} \frac{(\sin\theta)\, dt}{R}\right)\right] dt \tag{10c}$$

where θ is the surface gradient as shown in Fig. 7, V_{XL} and V_{YL} are micropart velocities in the local coordinate system, and dt is the simulation time step size. The local Z-axis is always perpendicular to the surface, therefore the velocity along the local Z-axis (V_{ZL}) is zero as long as the micropart stays on the surface. The effective change in position along the local Z-axis, as represented in (8), is due to the velocity component V_{YL} of the micropart along the curvature. For limiting cases when $\theta \to 0°$, the convergence for (10b) and (10c) is proven using L'Hospital's rule with converged values of $\Delta Y_L \to V_{YL} dt$ and $\Delta Z_L \to 0$.

Equations (10b) and (10c) are based on the observation that the tangential component of velocity V_{YL} on a curved surface will move an object along the local Y and Z directions simultaneously. The distance covered by the micropart due to the tangential component of the velocity, V_{YL}, is calculated by estimating the angle incurred by the micropart in a single simulation time step at the center of curvature. Let S be the length of the curved path due to V_{YL} and ψ the angle incurred by V_{YL}. The relations between S, ψ, radius of curvature R and time span dt are given by

$$S = R\psi \quad S = V_{YL} dt \quad \psi = \frac{V_{YL} dt}{R} \tag{11}$$

$$\Delta Y_L = R \sin\psi = R \sin\left(\frac{V_{YL} dt}{R}\right) \tag{12}$$

For a surface with gradient θ, (12) is updated to (10b) by replacing R with $R/sin\theta$ in (12). The division by $sin\theta$ defines the radius of curvature in terms of its projection on the horizontal plane.

B. IMPLEMENTATION OF NUMERICAL SIMULATION SCHEME

The stick-slip behavior during microscale movement is evaluated by considering a fixed time step to evaluate the micropart motion on the surface. The initial position of micropart is recorded and system states are transformed from the global to the local coordinate system. The predefined time-varying actuator position (quintic motion profile) is used to calculate the instantaneous value of inertia which is resolved into components along and perpendicular to the workcell surface. The component of inertia perpendicular to the surface is used to estimate the instantaneous friction force. The magnitude of the friction force is dynamically evaluated at each time step and its maximum value depends on surface and material properties. The direction of the friction force is calculated by estimating the direction of relative velocity between the micropart and workcell surface. The location of the micropart in the global coordinate system is updated using the system inertia, the instantaneous values of friction force and micropart velocity. The placement of micropart on the surface is ensured by comparing the normal component of system inertia with the force of attraction between micropart and workcell surface. After updating the micropart location, the process is repeated for the next time step. The block diagram highlighting the major components of the numerical simulation scheme to implement the algorithm for micropart motion profile is shown in Fig. 10.

V. VERIFICATION OF DEVELOPED NUMERICAL SIMULATION SCHEME

The developed solution sequence is used to simulate the micropart motion on a flexible surface. Benchmark test cases with specific initial conditions are used to validate the numerical scheme. These test cases include tracking of micropart motion on a surface for various initial locations of the micropart. The material properties and surface roughness values used for the analysis are shown in Table 1. The details of these test cases along with the basis of relevant verification for each case are discussed in the following subsections. The actuator motion profile for all verification cases is quintic [16].

A. CONFIRMATION OF STATE TRANSFORMATION

The transformation between the global and local coordinates and the micropart motion pattern are verified for various initial locations and zero initial velocity using a single actuator. The radially symmetric deformation due to a single actuator will push the part along the radial direction in deformation topology. Motion in the radial direction occurs when the velocity along one of the axes is a constant multiple of the velocity along other axis; i.e. they exhibit similar but

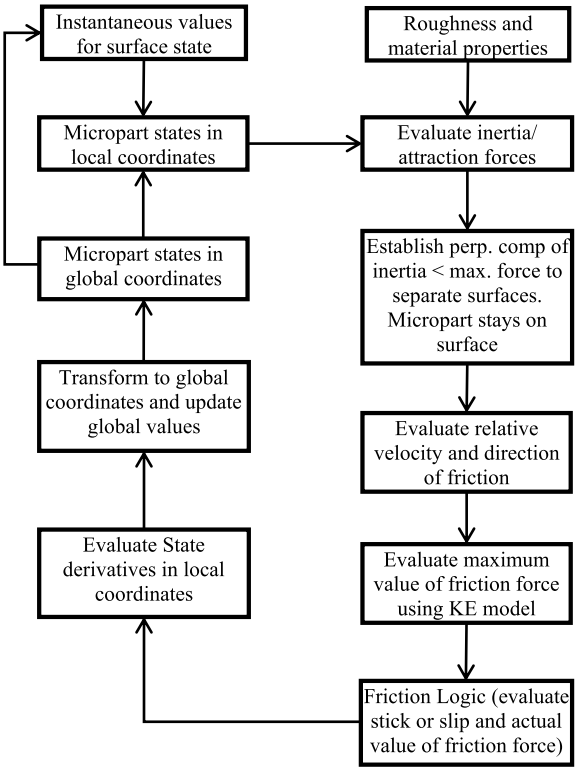

FIGURE 10. Numerical scheme to evaluate micropart state.

TABLE 1. Material and surface properties.

Description	Variable	Value
Standard deviation of surface roughness	σ	$20nm$
Micropart surface contact area	A_n	$100\mu m \times 100\mu m$
Poisson's ratio	ν	0.3
Plasticity index of surface and part [29], [30]	ψ	2.5
Adhesion energy [29], [30]	$\Delta\gamma$	$1Joule/m^2$
Hardness of material [30]	H	$200HB$
Micropart mass	m	$2 \times 10^{-9}Kg$

Note: here ψ represents the plasticity index and is independent of the angle variable used in the motion formulation.

instantaneously scaled profiles. The velocity components as function of time for a single actuator operating at $150\mu m$ stroke length and 1.6 *KHz* frequency are shown in Fig. 11. The velocity profiles are similar but scaled or offset relative to each other at any time instant which is an indicator of correct transformation between the global and local coordinates.

The micropart motion along the deformed surface is verified by plotting its coordinates relative to each other. The position of the micropart is plotted for the same test case of a single actuator and since the active surface deformation is radially symmetric, the position gradient is expected to be a straight line passing through the actuator location. Therefore, the time-dependent position plot should form a straight

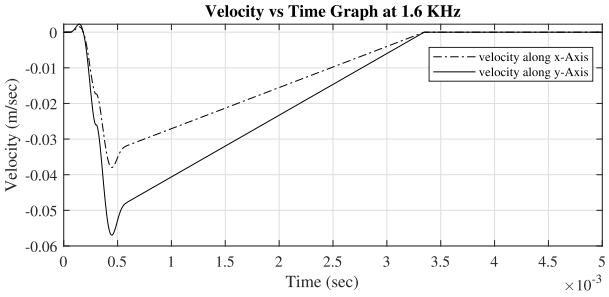

FIGURE 11. X and Y components of micropart velocity in global coordinate system.

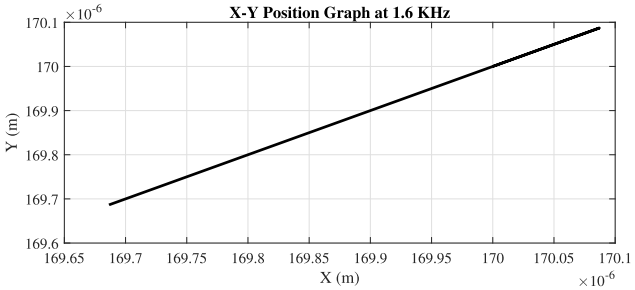

FIGURE 12. Micropart position graph along *X* and *Y* axes.

line as the trace in Fig. 12 which shows the motion profile of micropart for zero initial velocity and initial location of $(x, y) = (170.08, 170.08)\mu m$.

B. ACCURATE ESTIMATION OF FRICTION FORCE DURING SURFACE MOTION

The magnitude of the friction force is a function of the normal component of inertia whereas its direction depends on the relative velocity between the micropart and surface. Note, the relative velocity is evaluated in local coordinates and the actuator input is defined in global coordinates. The micropart acceleration (magnitude and direction) in global coordinates must be consistent with the accurate evaluation of friction force estimated in local coordinates and transformed to global coordinates. The accurate estimation of the friction force in the developed numerical scheme is performed by evaluating the micropart motion starting from rest (zero initial velocity) due to a single actuator stroke. Fig. 13 and Fig. 14 present the velocity versus time plots for two different initial locations of the micropart.

The initial phase of these plots (up to point *A*) shows the micropart acceleration due to imparted acceleration by actuator stroke and opposing friction force, whereas in the later phase, the micropart continues its motion due to attained velocity in the initial phase. Analyzing the later phase for both plots, the straight line velocity profile in global coordinates shows constant acceleration which indicates that the micropart is moving under constant opposing force. The actuator, operating at 1.6 *KHz* frequency, completes its stroke

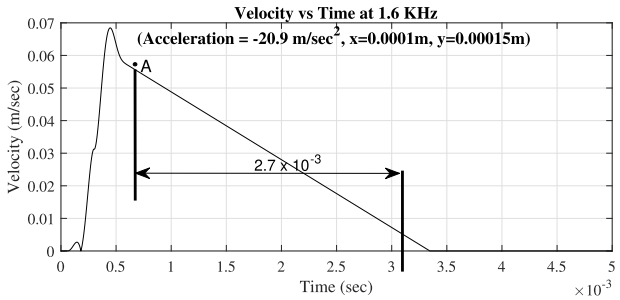

FIGURE 13. Velocity vs. time for initial location 1.

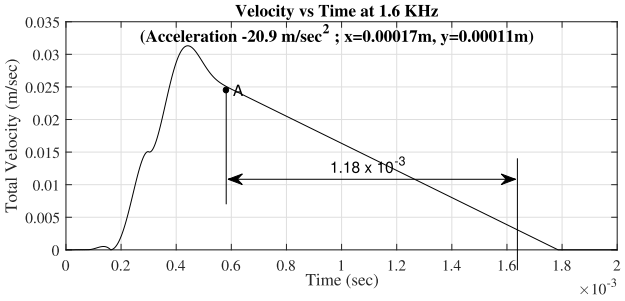

FIGURE 14. Velocity vs. time for initial location 2.

at $0.625 \times 10^{-3}s$. After this time, no inertia is imparted by the actuator and the only force affecting the micropart acceleration (deceleration) is the friction force. In the later part of the motion profile, the friction force stays constant. In addition, the value of acceleration calculated from both plots is $-20.9\ m/s^2$ which is the same value as the one predicted by the friction model using (3-5).

VI. RESULTS AND DISCUSSION

The verified numerical scheme and algorithm were employed to estimate the qualitative and quantitative behavior of microscale translocation for a single actuator and multi-actuator workcell. The translocation characteristics include the analysis of translocation distance, motion patterns on the surface, the position convergence and the placement accuracy of micropart at a specific location on the workcell surface.

A. MICROPART MOTION ON SURFACE DUE TO SINGLE ACTUATOR

The effect of the actuator stroke and frequency on translocation distance are studied for a range of input frequencies and strokes. The results are presented in Fig. 15 where each line represents the translocation distance for a constant actuator stroke for a range of input frequencies. The lower frequency values for each stroke set represent the frequency below which micropart motion is not possible since the imparted inertia cannot overcome the friction force. The upper frequency value for each stroke set represents the maximum

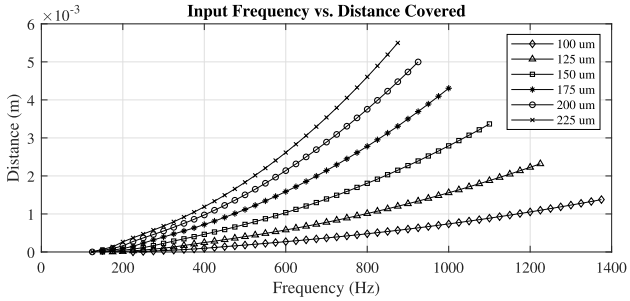

FIGURE 15. Distance travelled as function of input frequency and actuator stroke.

frequency at which motion is possible and beyond which the micropart detaches from the surface. Micropart translocation can only take place when considering both the frequency and stroke of the actuator; the information in Fig. 15 could be used to identify a range of actuator motion characteristics (frequency and stroke) for a desired translocation distance. The active surface deformation due to a single actuator is a radially symmetric problem and as such the observed motion trends are very similar to those for the 1D motion [16].

B. MICROPART MOTION ON MULTI-ACTUATOR WORKCELL

A single actuator with zero initial velocity of the micropart, due to symmetry in the deformation profile, generates a straight line motion on the surface but a more viable workcell must be capable of controlling the micropart motion in any direction. The developed algorithm is employed to estimate the functionality and operation of a multi-actuator workcell and evaluate the translocation path for different initial states (location and velocity) of the micropart. An array of two actuators placed $150\mu m$ relative to each other in the workcell is used for this analysis. This actuator spacing is approximately 33% of the deformation wavelength [17]. In this analysis, both actuators are operating with the same stroke length and frequency. The stroke length is $150\mu m$ however, the frequency is varied from 250 to 650 Hz in order to evaluate its effect on the micropart path. The path of the micropart on the 2D surface for various input frequencies is shown in Fig. 16.

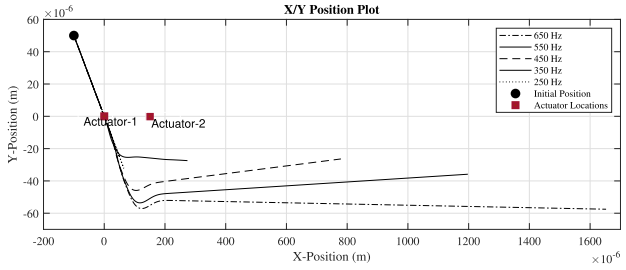

FIGURE 16. Micropart motion on a 2D surface for a range of input frequencies with constant stroke of $150\mu m$.

The analysis of Fig. 16 at the low frequency of 250 Hz shows that the micropart moved from its initial location, reached actuator-1, crossed it and then came back in the region of same actuator. Contrary to this, at higher frequency, the micropart translocates towards neighboring actuators which will define its subsequent movement. The micropart motion patterns in Fig. 16 show the possibility of large translocation and different path motion on the 2D surface. These translocation patterns reveal two distinct trends due to changes in the input frequency:

a) micropart converges to certain locations on the workcell,
b) micropart leaves certain areas.

These results demonstrate the motion of the micropart could be furthered controlled by the actuation characteristics of a neighboring actuator and the initial state (rest or moving) of the micropart. As such, considering an actuator array, the motion and path characteristics of a micropart could be controlled on a 2D plane by properly engaging and controlling the appropriate actuator motion characteristics.

C. MICROPART POSITION CONVERGENCE: SINGLE STROKE

In the presented example in VI-B, the two actuators operated at a fixed stroke. In a general purpose workcell, a controlled number of actuator strokes considering the state of the micropart might not be practical. A different approach that would allow the translocation of the micropart from any location to a specific location will be to define the actuator frequency and operate the actuator in a continuous fashion to achieve micropart position convergence. The possibility of position convergence employing this approach is investigated on a 2D surface using a single actuator (undergoing continuous strokes) and a range of input frequencies. The micropart motion paths are shown in Fig. 17a and b where two distinct trends of convergence and non-convergence are observed. The micropart initial location at (100, 100)μm and the actuator stroke of 150μm are kept the same for both cases with the only difference being the input frequency of 300 Hz and 600 Hz. In Fig. 17a at 300 Hz, under repeated actuator strokes, the micropart starts moving from rest, undergoes to-and-fro motion and converges at the neighboring actuator located at (0, 0). In Fig. 17b at 600 Hz, in two actuator strokes, the micropart leaves the region of influence of the actuator. In addition, the path of the micropart in the 2D plane for each case is also presented.

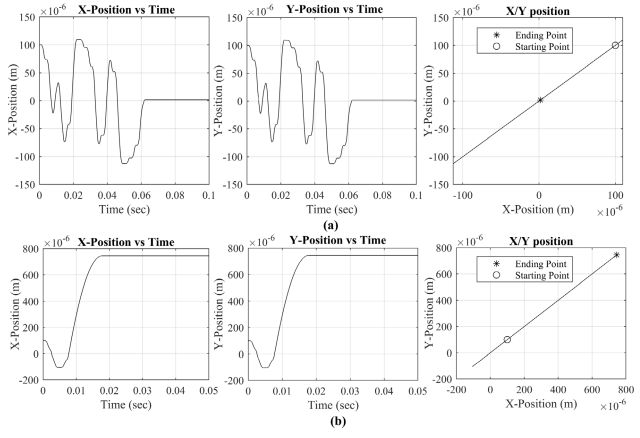

FIGURE 17. Micropart motion starting at same initial location and actuator stroke; (a) at 300 Hz micropart converges to the neighboring actuator at the origin and (b) at 600 Hz the micropart leaves the high frequency actuator region.

Estimating the micropart motion at various input frequencies, the threshold frequency is estimated to be 320 Hz for an actuator stroke of 150μm at continuous operation. Below this threshold value, the micropart will converge to the actuator whereas at higher frequency, micropart will exhibit larger translocation and will leave the region of influence of the actuator. The threshold frequency for continuous operation is a function of stroke length and is evaluated for various stroke lengths ($100 - 200\mu m$). The results of the evaluation indicate a quadratic relationship and are presented in Fig. 18.

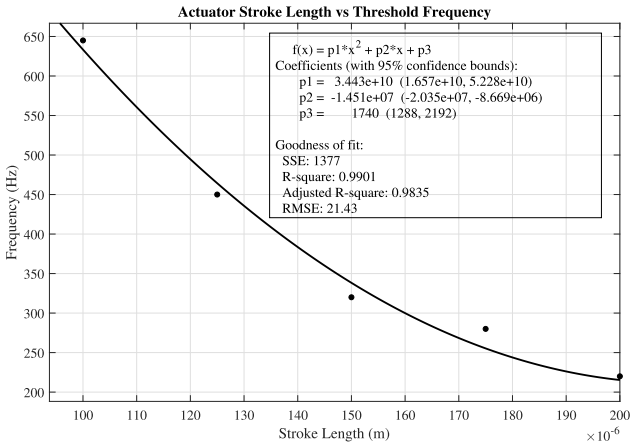

FIGURE 18. Effect of actuator stroke length on threshold frequency.

The micropart convergence due to a single actuator under repeated strokes opens the possibility of convergence on a multi-actuator 2D surface, not only for certain initial locations but rather when the micropart is initially placed at any location on the workcell will leave the high frequency region and converge to low frequency areas. Fig. 17 shows the micropart convergence with zero initial velocity. However, in a workcell, the micropart will not always have zero initial velocity since while leaving the high frequency regions the micropart will have non-zero velocity for engaging with the subsequent actuators. In order to validate the micropart convergence for any initial state, micropart movement is examined for a single actuator for various initial locations and non-zero initial velocities with the convergence plots of micropart shown in Fig. 19.

D. GENERAL CONVERGENCE OF MICROPART ON WORKCELL

After verifying micropart convergence at low frequency region with a single actuator, the micropart motion on a

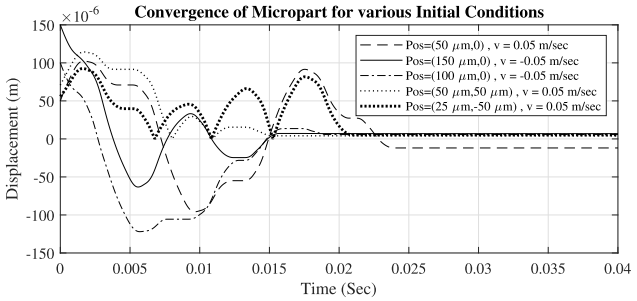

FIGURE 19. Convergence of micropart on 2D surface for various initial states (location and velocity) at a frequency of 250 *Hz* and a stroke length of 150μm.

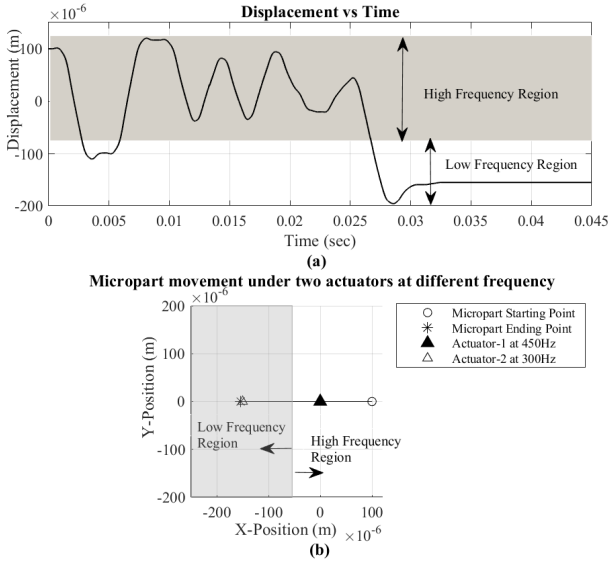

FIGURE 20. Convergence of micropart from region of high frequency (450 *Hz*) to that of low frequency (300 *Hz*) actuator; actuators are located 150μm apart.

workcell of two actuators continuously operating at different frequencies is estimated. The high and low operating frequencies are defined at 450 Hz and 300 Hz respectively with a stroke of 150μm. The neighboring actuators are located 150μm apart. The initial location of micropart is at $(100, 0)\mu m$, and in the region of the high frequency actuator as shown in Fig. 20. The results presented in Fig. 20 indicate that after five oscillations of the high frequency actuator the micropart leaves the high frequency region (shaded gray) and reaches the region of the low frequency actuator operating at 300 Hz. The location map and path of the micropart due to the motion of both actuators are shown in Fig. 20b.

In Fig. 20, the micropart movement is along the straight line on a surface since the three locations, those of the micropart (initial state) and actuators A and B are along a straight line. To ensure general convergence, the path is calculated for a general scenario where the micropart and actuators are not along a straight line. The results are shown in Fig. 21 where two actuators, placed 150μm apart, operating

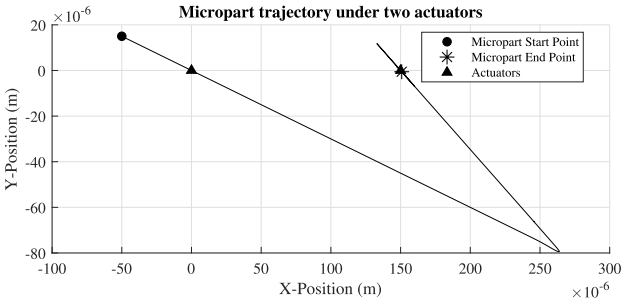

FIGURE 21. XY path of micropart motion where the micropart converges in the region of low frequency actuator.

continuously at 400 Hz and 300 Hz, push the micropart to converge in the low frequency region. The XY map shows the micropart motion starting from rest and at initial location $(-50, 15)\mu m$ and ending at $(150, 0)\mu m$. The micropart motion is due to the active surface deformation induced by both actuators. The starting and ending locations are also shown on the XY map of the surface.

E. MICROPART PLACEMENT ACCURACY

In this subsection, the effect of micropart initial state (position and velocity) and actuation parameters (frequency and stroke) on the accuracy of placing the micropart at a desired location is evaluated. The desired placement location is the actuator location at $(0, 0)$. This accuracy is evaluated only for a specific set of controllable actuator parameters used in the numerical analysis of this research. A frequency range of (240 to 320)Hz in discrete increments of 10 Hz and a single actuator in continuous operation with a stroke length of 150μm are used. The results of the study are presented in Fig. 22. It is observed that the placement accuracy is a function of micropart initial state and actuation parameters. The accuracy for the set of parameters considered is within a band of $\pm 5\mu m$. It is also observed that for certain combinations of the parameters, the placement accuracy was less than 1μm; for example, starting from rest placed

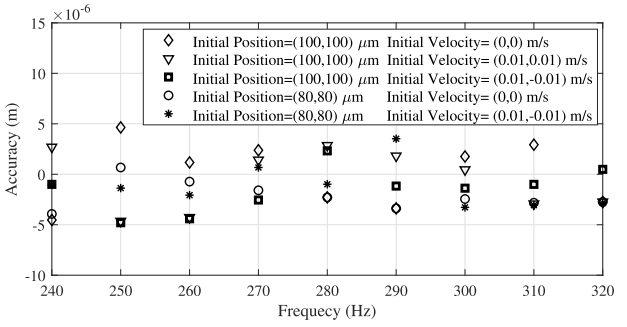

FIGURE 22. Micropart placement accuracy for a set of initial states (position and velocity) and a range of frequencies with a fixed actuator stroke value of 150μm.

at $(80, 80)\mu m$ for frequency 250 Hz or starting with initial velocity of $(0.01, 0.01)m/s$ placed at $(100, 100)\mu m$ for frequency 300 Hz.

The results of this analysis prove that an improved placement accuracy could be achieved through an optimization process to estimate better combinations of actuator frequency and stroke length. However, an optimization is beyond the scope of this manuscript which aims to establish the feasibility of an active surface based workcell.

VII. LIMITATION OF STUDY

We have presented the theoretical system model and developed the dynamics and analysis demonstrating the feasibility of both motion and placement of the micropart at a desired region employing the active surface concept. All relevant microscale forces have been considered in the developed model. The proposed methodology has not been verified with experimental data. However, the results of any future experimental work will be presented and compared with the predicted theoretical ones.

VIII. CONCLUSION

Translocation and/or motion of microparts $\sim 10^{-9} Kg$ is possible by employing a controllably deformed or excited continuous surface. The ensuing motion is a function of physical properties of the micropart, surface roughness, micropart initial state, as well as the spacing and motion characteristics (frequency and stroke) of the actuators employed to deform the surface. The placement and capabilities of the actuators avoid dead zone constraints by considering the actuator feasible region of influence in their spacing which depends on actuator motion characteristics.

The feasibility of micropart motion and placement was demonstrated by simulating the developed model using a 2D active surface deformed by two actuators. It was found that the micropart motion may converge or diverge from specific regions depending on the actuator motion characteristics (frequency and stroke) and micropart initial state. In the range of motion characteristics examined in this research, a general placement accuracy band of $\pm 5\mu m$ was achieved.

The placement accuracy of the micropart and the operating parameters of the actuators found in this research demonstrate the possible realization of a workcell or microconveyor platform comprising of a properly arranged cascaded actuator array based on the 2D active surface concept for controlled manipulation and translocation of microparts.

REFERENCES

[1] B.-S. Kim, J.-S. Park, B. Hun Kang, and C. Moon, "Fabrication and property analysis of a MEMS micro-gripper for robotic micro-manipulation," *Robot. Comput.-Integr. Manuf.*, vol. 28, no. 1, pp. 50–56, Feb. 2012.

[2] R. Zhang, J. Chu, H. Wang, and Z. Chen, "A multipurpose electrothermal microgripper for biological micro-manipulation," *Microsyst. Technol.*, vol. 19, no. 1, pp. 89–97, Jan. 2013.

[3] V. Vandaele, P. Lambert, and A. Delchambre, "Non-contact handling in microassembly: Acoustical levitation," *Precis. Eng.*, vol. 29, no. 4, pp. 491–505, Oct. 2005.

[4] M. Gauthier, *Microhandling Strategies and Microassembly in Submerged Medium*. Hoboken, NJ, USA: Wiley, 2011, ch. Robotic Microassembly, pp. 189–224.

[5] H. M. El-Badry, *Micromanipulators and Micromanipulation*, vol. 3. USA: Springer, 2012, ch. Micromanipulators.

[6] T. Furuhata, T. Hirano, and H. Fujita, "Array-driven ultrasonic microactuators," in *TRANSDUCERS, Int. Conf. Solid-State Sens. Actuators. Dig. Tech. Papers*, Jun. 1991, pp. 1056–1059.

[7] J. W. Suh, S. F. Glander, R. B. Darling, C. W. Storment, and G. T. A. Kovacs, "Combined organic thermal and electrostatic omnidirectional ciliary microactuator array for object positioning and inspection," in *Proc. Solid State Sensor Actuator Workshop*, Jun. 1996, pp. 168–173.

[8] H. Fujita, M. Ataka, and S. Konishi, "Cooperative work of arrayed microactuators," in *Proc. IECON 20th Annu. Conf. IEEE Ind. Electron.*, Sep. 1994, pp. 1478–1482.

[9] K. S. J. Pister, R. S. Fearing, and R. T. Howe, "A planar air levitated electrostatic actuator system," in *Proc. IEEE Micro Electro Mech. Syst., Invest. Micro Struct., Sensors, Actuat., Mach. Robots*, Feb. 1990, pp. 67–71.

[10] J. D. Jacobson, S. H. Goodwin-Johansson, S. M. Bobbio, C. A. Bartlett, and L. N. Yadon, "Integrated force arrays: Theory and modeling of static operation," *J. Microelectromech. Syst.*, vol. 4, no. 3, pp. 139–150, Sep. 1995.

[11] H. Skima, E. Dedu, J. Bourgeois, C. Varnier, and K. Medjaher, "Optimal path evolution in a dynamic distributed MEMS-based conveyor," in *Proc. Int. Conf. Dependability Complex Syst.* Cham, Switzerland: Springer, 2016, pp. 395–408.

[12] H. Mabed, E. Dedu, and H. Skima, "Multicriteria optimization in distributed micro-conveying platform," in *Proc. Symp. Appl. Comput.*, Apr. 2017, pp. 241–248.

[13] V. Ruiz-Díez, J. Hernando-García, J. Toledo, A. Ababneh, H. Seidel, and J. L. Sánchez-Rojas, "Bidirectional linear motion by travelling waves on legged piezoelectric microfabricated plates," *Micromachines*, vol. 11, no. 5, p. 517, May 2020.

[14] Q. Zhou, V. Sariola, K. Latifi, and V. Liimatainen, "Controlling the motion of multiple objects on a Chladni plate," *Nat. Commun.*, vol. 7, no. 12764, pp. 1–10, 2016.

[15] R. Yahiaoui, R. Zeggari, J. Malapert, and J.-F. Manceau, "A MEMS-based pneumatic micro-conveyor for planar micromanipulation," *Mechatronics*, vol. 22, no. 5, pp. 515–521, Aug. 2012.

[16] M. Rizwan and P. S. Shiakolas, "Motion analysis of micropart in dry friction environment due to surface excitation considering microscale forces," *J. Tribol.*, vol. 133, no. 4, Oct. 2011.

[17] M. Rizwan and P. S. Shiakolas, "Sensitivity analysis of micropart motion on a controlled deformable continuous surface," in *Proc. ASME Int. Mech. Eng. Congr. Expo.*, vol. 9, 2012, pp. 319–326.

[18] S.-A. Zhou, "On forces in microelectromechanical systems," *Int. J. Eng. Sci.*, vol. 41, nos. 3–5, pp. 313–335, Mar. 2003.

[19] Y. Rollot, S. Régnier, and J.-C. Guinot, "Simulation of micromanipulations: Adhesion forces and specific dynamic models," *Int. J. Adhes. Adhesives*, vol. 19, no. 1, pp. 35–48, Feb. 1999.

[20] L. Kogut and I. Etsion, "A static friction model for elastic-plastic contacting rough surfaces," *J. Tribol.*, vol. 126, no. 1, pp. 34–40, Jan. 2004.

[21] C. R. Steele and C. D. Balch, "Introduction to the theory of plates," Division Mech. Comput., Dept. Mech. Eng., Stanford Univ., Stanford, CA, USA, 2009. [Online]. Available: http://web.stanford.edu/~chasst/Course%20Notes/Introduction%20to%20the%20Theory%20of%20Plates.pdf

[22] L. Kogut and I. Etsion, "Adhesion in elastic–plastic spherical microcontact," *J. Colloid Interface Sci.*, vol. 261, no. 2, pp. 372–378, May 2003.

[23] L. Kogut and I. Etsion, "A semi-analytical solution for the sliding inception of a spherical contact," *J. Tribol.*, vol. 125, no. 3, pp. 499–506, Jul. 2003.

[24] L. Kogut and I. Etsion, "Elastic-plastic contact analysis of a sphere and a rigid flat," *J. Appl. Mech.*, vol. 69, no. 5, pp. 657–662, 2002.

[25] M. Rizwan and P. S. Shiakolas, "On the acceleration limits for sliding and detachment between contacting rough surfaces for micropart manipulation in a dry environment," *J. Micro Nano-Manuf.*, vol. 1, no. 1, pp. 1–8, Mar. 2013.

[26] N. V. Zarate, A. J. Harrison, J. D. Litster, and S. P. Beaudoin, "Effect of relative humidity on onset of capillary forces for rough surfaces," *J. Colloid Interface Sci.*, vol. 411, pp. 265–272, Dec. 2013.

[27] K. Wendler, J. Thar, S. Zahn, and B. Kirchner, "Estimating the hydrogen bond energy," *J. Phys. Chem. A*, vol. 114, no. 35, pp. 9529–9536, Sep. 2010.

[28] P. E. M. Lopes, B. Roux, and A. D. MacKerell, "Molecular modeling and dynamics studies with explicit inclusion of electronic polarizability: Theory and applications," *Theor. Chem. Accounts*, vol. 124, nos. 1–2, pp. 11–28, Sep. 2009.

[29] W. R. Chang, I. Etsion, and D. B. Bogy, "An elastic-plastic model for the contact of rough surfaces," *J. Tribol.*, vol. 109, no. 2, pp. 257–263, Apr. 1987.
[30] W. R. Chang, I. Etsion, and D. B. Bogy, "Adhesion model for metallic rough surfaces," *J. Tribol.*, vol. 110, no. 1, pp. 50–56, Jan. 1988.

MUHAMMAD AHSAN NAEEM received the B.S. and M.S. degrees in electrical engineering from the Department of Electrical Engineering, University of Engineering and Technology (UET), Lahore, Pakistan, in 2007 and 2013, respectively, where he is currently pursuing the Ph.D. degree in mechatronics with the Department of Mechatronics and Control Engineering.

From 2009 to 2014, he was a Lecturer with the Department of Mechatronics and Control Engineering, UET, where he has been working as an Assistant Professor, since 2014. His research interests include modeling of MEMS, control systems, and embedded systems.

MOHSIN RIZWAN received the B.S. degree from the Department of Mechanical Engineering, University of Engineering and Technology (UET), Lahore, Pakistan, and the Ph.D. degree from The University of Texas at Arlington, Arlington, TX, USA, in 2011. He is currently working as an Associate Professor with the Department of Mechatronics and Control Engineering, UET. His current research interests include system modeling, MEMS, and the design and analysis of feedback control systems.

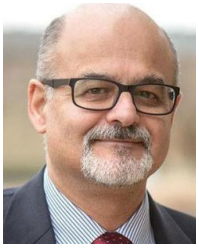

P. S. SHIAKOLAS received the Higher National Diploma degree from the Higher Technical Institute, Nicosia, Cyprus, in 1982, the B.S. and M.S. degrees from The University of Texas at Austin, in 1986 and 1988, respectively, and the Ph.D. degree from The University of Texas at Arlington (UTA), in 1992, all in mechanical engineering in the areas of robotics and computer aided design. From 1993 to 1996, he worked as a Faculty-Research Associate with UTA. He joined the UTA Faculty as an Assistant Professor, in 1996, where he currently serves as a Tenured Associate Professor for mechanical and aerospace engineering. He is also the Director of the MARS Laboratory, UTA. His research interests include generals areas of robotics, manufacturing, microsystems, automation, and controls as they apply to the betterment of society currently focusing in the medical/biomedical fields. He has a passion for engineering education and he has developed educational testbeds and routinely uses hardware testbeds to demonstrate concepts in his courses in the areas of robotics, automation, and controls.